

# Ozone Monitoring Instrument in-flight performance and calibration

M. Dobber<sup>\*a</sup>, R. Dirksen<sup>a,b</sup>, P. Levelt<sup>a</sup>, B. van den Oord<sup>a</sup>, R. Voors<sup>a</sup>, Q. Kleipool<sup>a</sup>,  
G. Jaross<sup>c</sup>, M. Kowalewski<sup>c</sup>

<sup>a</sup>Royal Netherlands Meteorological Institute, PO Box 201, 3730 AE De Bilt, NL, dobber@knmi.nl;

<sup>b</sup>Space Research Organisation Netherlands, Sorbonnelaan 2, 3584 CA Utrecht, NL;

<sup>c</sup>Science systems & Applications Inc, GSFC-Code 916, Greenbelt, MD USA 20771

## ABSTRACT

The Ozone Monitoring Instrument (OMI) was launched on 15 July 2004 on NASA's EOS AURA satellite. The OMI instrument is an ultraviolet-visible imaging spectrograph that uses two-dimensional CCD detectors to register both the spectrum and the swath perpendicular to the flight direction with a 115 degrees wide swath, which enables global daily ground coverage with high spatial resolution. This paper presents a number of in-flight radiometric and spectral instrument performance and calibration results.

**Keywords:** calibration, remote sensing, charge coupled devices, ultraviolet spectroscopy.

## 1. INTRODUCTION

The primary objective of the OMI instrument on the EOS-AURA satellite is to obtain daily global measurements of ozone and nitrogen dioxide in both the troposphere and stratosphere. The central science issues addressed by the OMI mission are the recovery of the ozone layer, the depletion of ozone at the poles, tropospheric pollution and climate change. In addition, OMI is intended as the successor to the Total Ozone Mapping Spectrometer (TOMS) operated by NASA over the past 25 years.<sup>1</sup>

OMI combines a high spatial resolution and daily global coverage. In this way tropospheric trace gases can be observed with high spatial resolution and cloud-free ground pixels are more easily obtained as compared to instruments with scanning mirrors. OMI will deliver absolutely calibrated spectral radiances and irradiances in the spectral range from 264-504 nm. These are used to retrieve the primary data products: ozone total column, ozone vertical profile, UV-B flux, nitrogen dioxide total column, aerosol optical thickness, cloud effective cover, cloud top pressure and secondary data products: total column SO<sub>2</sub>, BrO, HCHO and OCIO. The atmospheric constituent concentrations are retrieved from nadir observations of backscattered light from the sun on the earth's atmosphere in the ultraviolet-visible wavelength range (264-504 nm). Both Differential Optical Absorption Spectroscopy (DOAS) and algorithms that have been used before in the TOMS instrument series for the retrieval of total columns of the various atmospheric constituent concentrations are used.<sup>2,3</sup> The ozone profile is obtained from strong wavelength dependence of the absorption cross-section between 270 and 330 nm. The retrieval methods used for predecessor instruments like the Global Ozone Monitoring Instrument (GOME) on ERS-2, the Scanning Imaging Absorption Spectrometer for Atmospheric Cartography (SCIAMACHY) on ENVISAT, TOMS and Solar Backscatter UltraViolet (SBUV) are also applied to OMI measurement data.

The integration of the OMI proto-flight model (PFM) was completed in 2001. This was followed by an extensive performance verification program, which has proven that the OMI instrument is compliant to all requirements. Subsequently, an extensive on-ground calibration measurement campaign was performed from April - November 2002. During this calibration period measurements were performed under both ambient and in-flight representative thermal-vacuum conditions. After conclusion of the calibration period the OMI instrument was shipped to the U.S. for integration on the EOS-AURA spacecraft. Extensive testing on spacecraft level was performed from November 2002 until March 2004. The satellite with OMI on board was successfully launched from the Vandenberg Air Force Base on 15 July 2004. Subsequently a three month in-orbit check-out and performance verification period was started, called the Launch and Early Operations Phase (LEOP). During this period various dedicated measurements were performed. The in-orbit functional performance of the OMI instrument was found to be as expected from pre-launch testing. During the

initial four weeks of the mission in orbit, the temperature of the optical bench and the detectors was increased to 303 K for optimal outgassing conditions. Subsequently the temperatures were lowered to their operational values at 264 K (optical bench) and 265 K (detectors). After that the temperature was increased to 303 K and lowered again on two more occasions during the LEOP for a duration of one week each time. The nominal operations phase was started on 27 September 2004.

For remote sensing instruments like OMI a good on-ground calibration delivering reliable calibration key data for 0-1 data processing, as well as an extensive and continuous in-flight calibration, are essential to meet the required accuracies for the target scientific data products, especially when the data is to be compared to and to become part of long-term ozone trend records. The OMI in-flight calibration was started immediately after launch in the LEO phase and has as main goals to verify the in-orbit calibration status of the instrument compared to the pre-launch calibration, to investigate if unanticipated behaviour occurs in flight and to keep the calibration accuracy of the instrument up-to-date as a function of time, i.e. monitor and correct for potential changes that may occur in flight. The in-flight calibration is an activity that continues until the end of the mission, with an anticipated lifetime of five years. A number of pre-flight and in-flight radiometric and spectral calibration results for OMI are presented and discussed below.

OMI has been developed by Dutch and Finnish industry in close collaboration with the climate research and meteorological community and under contract with the Netherlands Agency for Aerospace Programmes (NIVR) and the Finnish Meteorological Institute (FMI). The Royal Netherlands Meteorological Institute (KNMI) is the Principal Investigator (PI) institute for the OMI instrument.

## 2. OMI INSTRUMENT DESCRIPTION

The OMI instrument is a compact nadir viewing ultraviolet-visible imaging spectrograph with two spectral channels, each having a two-dimensional frame transfer CCD. The 115 degrees large field-of-view perpendicular to the flight direction yields a 2600 km wide ground swath that is wide enough to obtain daily global coverage of the earth's atmosphere at the equator. The swath is sampled by 60 (electronically binned) pixels. The size of a pixel projected on the earth's surface is  $13 \times 24 \text{ km}^2$  (flight direction  $\times$  swath direction) in the nadir direction. The pixels close to the edge of the swath become progressively larger. By employing a two-dimensional CCD the spectrum of every ground pixel is recorded simultaneously. In one CCD dimension the spectrum is recorded, while the viewing direction is recorded in the other dimension. The operational temperature of the optical bench is 264 K and the temperature of the CCD detectors is stabilised at a temperature of 265 K.

A layout of the OMI optical bench depicting the telescope and the UV optical channel is presented in fig. 1, where the large 115 degrees swath is perpendicular to the plane of the paper. The telescope, consisting of a primary mirror, a polarisation scrambler and a secondary mirror, focuses the incident radiance on the entrance slit 008. The telescope is  $f/15$  in the flight direction and  $f/11$  in the swath direction. The entrance aperture 001, which is only about  $9 \text{ mm}^2$  in area in order to suppress spatial stray light, does not limit the field or aperture. The polarisation scrambler makes the instrument insensitive to the polarisation state of the incoming radiance, which simplifies the calibration of the instrument considerably. Note that the aluminium primary telescope mirror 003 is located before the polarisation scrambler, thus introducing a potential polarisation dependence of the instrument. However, the polarisation introduced by the primary telescope mirror is cancelled almost completely by the first uncoated surface of the polarisation scrambler. It has been verified by experiment that the polarisation dependence of the complete instrument to light with polarisation parallel and perpendicular to the entrance slit is less than 0.5%.

Solar irradiance enters the instrument through the solar port, which is equipped with a 10% transmission mesh, to illuminate one of three reflection diffusers (C04, C06, C06'). The solar port is closed by a shutter when not in use to protect the on-board diffusers. A folding mirror (C03) couples the diffuser signal into the main optical path just before the polarisation scrambler. An on-board white light source (WLS) can be coupled in through a transmission diffuser C05 and the same folding mirror C03. For on-ground calibration purposes this optical path was also used by mounting external stimuli on a calibration port close to the WLS. The light reflected from one of the on-board diffusers illuminates the full length of the spectrograph slit and thereby all viewing directions (CCD rows) within the field-of-view. Behind the entrance slit the main beam is split into two channels by dichroic mirror 009: the UV (264-383 nm) and the Visible (349-504 nm). The visible part of the spectrometer is shown in fig. 2. The UV channel is separated into two sub-channels, UV1 (264-311 nm) and UV2 (307-383 nm), in order to suppress stray light at ultraviolet wavelengths and in order to compensate for the significantly lower light fluxes from the earth below 300 nm as a result of ozone

absorption. Mirror 104 is segmented and has a spatially graded efficiency coating that reduces reflectance of higher wavelengths at the lower part of the mirror to reduce stray light at the low wavelengths (below 310 nm). The UV1 channel is scaled down by a factor two in both dimensions, meaning that both the spectral and spatial sampling distances are 2 times larger as compared to the UV2 sub-channel. This has been done to improve the signal-to-noise in the UV1.

The integration time of 2 seconds, consisting of co-added 0.4 s individual exposures, defines the spatial sampling in the flight direction to 13 km. The CCD detector has a frame transfer layout to allow simultaneous exposure and readout of the previous exposure, avoiding data loss during readout. In the nominal operational mode (global mode) eight CCD rows are electronically added (binned) during the readout. This decreases the contribution of the readout noise and the internal data rate, and increases the signal to noise. This sets the ground pixel size in the swath direction to 24 km. A number of OMI instrument properties are summarised in the table I. More details on the optical and electrical design of the OMI instrument and on operational and 0-1 data processing aspects can be found elsewhere.<sup>4,6</sup>

Table I: OMI instrument properties.

Spectral range	UV1: 264-311 nm UV2: 307-383 nm VIS: 349 – 504 nm
Spectral sampling	UV1: 0.33 nm / px UV2: 0.14 nm / px VIS: 0.21 nm / px
Spectral resolution (FWHM)	UV1: 1.9 px = 0.63 nm UV2: 3.0 px = 0.42 nm VIS: 3.0 px = 0.63 nm
Telescope swath IFOV	115 degrees (2600 km on the ground)
Telescope flight IFOV	1.0 degrees (12 km on the ground)
Ground pixel size global mode (electronic binning factor 8)	UV1: 13 km x 48 km UV2: 13 km x 24 km VIS: 13 km x 24 km
Ground pixel size spatial zoom-in mode (electronic binning factor 4)	UV1: 13 km x 24 km UV2: 13 km x 12 km VIS: 13 km x 12 km
Silicon CCD detectors	780 x 576 (spectral x spatial) pixels
CCD detector shielding	10 kg, about 40 mm thick aluminium
Operational CCD temperature	UV: 265.07 K VIS: 264.99 K
In-orbit CCD temperature excursion	UV and VIS: $\pm 10$ mK (stabilised)
Operational optical bench temperature	264 K
In-orbit optical bench temperature excursion	$\pm 300$ mK
Duty cycle	60 minutes on daylight side (Earth and Sun measurements) 10-30 minutes on eclipse side (calibration measurements)
Average data rate	0.8 Mbps
Power	66 Watts
Mass	65 kg
Size	50 cm x 40 cm x 35 cm
Orbit	Polar, sun-synchronous Average altitude: 705 km (438 mi) Orbit period: 98 minutes 53 seconds Ascending node local time: 1:42 PM

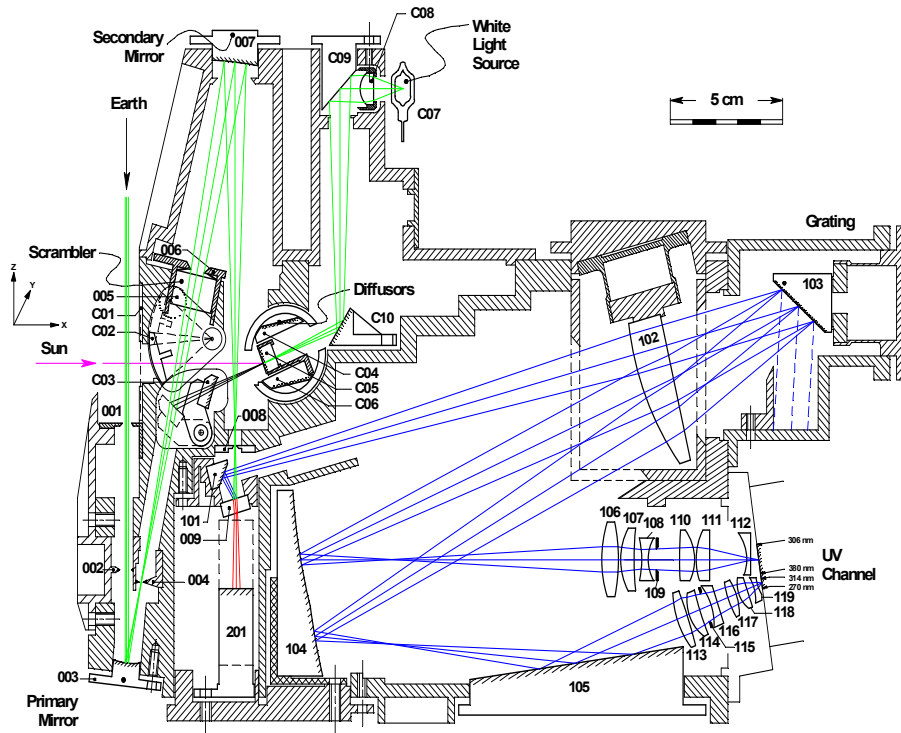


Fig. 1: Layout of the optical bench of the OMI instrument: telescope + ultraviolet spectral channel. The light beam passing through dichroic mirror 009 is reflected by mirror 201 to the visible channel.

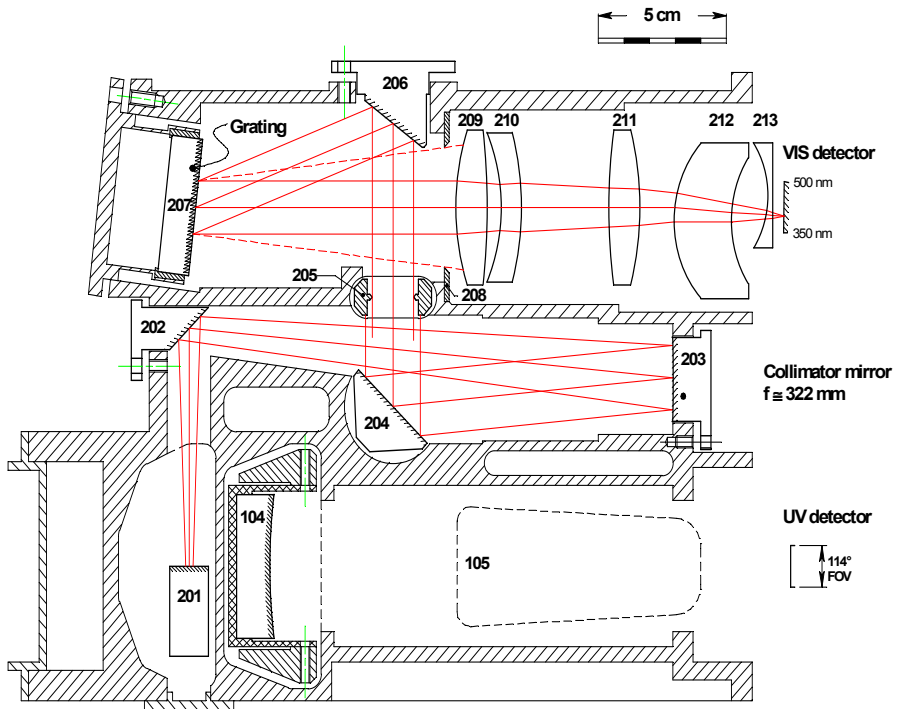


Fig. 2: Optical layout of the OMI visible (VIS) channel.

For in-flight calibration the OMI instrument is equipped with a number of possibilities. A set of three reflective diffusers (C04, C06, C06') for absolute radiometric calibration by daily measurement of the sun. Two of the three diffusers are ground aluminium diffusers, one used on a weekly basis, the other once per month to monitor the degradation of the first diffuser. The remaining diffuser is a quartz volume diffuser that is used on a daily basis. This diffuser is ground on both sides and aluminium coated on the backside. The term volume diffuser refers to the fact that the first ground surface is used as a transmission diffuser, while the second aluminium coated surface acts as a reflectance diffuser. Finally, the first surface acts once more as a transmission diffuser for the reflected beam. The thickness of the diffuser is about 6 mm. These multiple diffusive surfaces reduce the impact of surface structures. The volume diffuser was implemented, because ground aluminium diffusers exhibit wavelength dependent interference structures that affect the accuracy of the radiometric calibration and that have a detrimental impact on the DOAS retrieval of data products. As a result of its smooth surface and the multiple diffusive surfaces the spectral and spatial structures introduced by the volume diffuser are at least an order of magnitude smaller. The diffusers are well protected from contamination and solar irradiance by the solar aperture block C02 while not in use.

The white light source (WLS) C07 is used to monitor the pixel-to-pixel response non-uniformity calibration, the degradation of the detector (bad/dead pixels) and the instrument radiometric calibration, albeit it with limited accuracy (about 0.5%), because the lamp, its thermal environment and the power supply have not been designed to be radiometrically stable beyond this accuracy. For the WLS the transmission diffuser C05 is used to fill the entrance slit homogeneously.

Two green LEDs per (sub)channel are mounted in the proximity of the CCD detector to trace bad/dead pixels. Both the WLS and LEDs can be used in flight to monitor the detector plus electronics non-linearity.

At the eclipse side of the orbit the dark signal is measured accurately by performing both long exposure time dark measurements (exposure times 22, 78 and 136 seconds) and dark signal measurements with instrument settings identical to radiance measurements at the dayside of the orbit. The latter measurements are performed with the folding mirror C03 in the position that lets the earth light pass. In addition, once per week the same measurements are performed with the folding mirror C03 in blocking position in order to study spurious light contributions in the eclipse. The spectral calibration is performed using the solar Fraunhofer lines in solar and earth spectra.

### 3. RADIOMETRIC CALIBRATION

The radiometric calibration of the OMI instrument comprises the absolute radiance and irradiance calibration and the calibration of the instrument Bi-directional Spectral Distribution Function (BSDF), which is equal to the ratio irradiance over radiance calibrations. The radiance calibration depends on the swath angle viewing direction of 115 degrees and on wavelength. The irradiance calibration depends on the same parameters, as well as on the solar elevation and azimuth angles. The elevation angle changes with satellite movement in orbit over a range  $-4.0$  to  $+4.0$  degrees with a nominal value of 0.0 degrees. The azimuth angle changes with season from 18.5 to 31.5 degrees around a nominal value of about 26 degrees. The BSDF depends on swath angle, elevation and azimuth angles, diffuser and wavelength.

The optical layout presented in fig. 1 shows that the optical path for the radiance and the irradiance mode is identical except for the primary telescope mirror 003, that is unique for the radiance path, and the solar mesh, the on-board diffuser (C04, C06, C06') and the folding mirror C03, that are unique to the irradiance path. The other optical components in the OMI instrument are common for the (ir)radiance path and therefore cancel in first order in the ratio irradiance/radiance, which constitutes the instrument BSDF. Consequently the instrument BSDF includes the efficiency of the on-board diffuser, the solar mesh, and the primary and the folding mirror. The BSDF is the key parameter to calibrate the absolute earth reflectance. The absolute earth reflectance (the earth radiance divided by the solar irradiance) is the basic input for all level 1-2 data product retrieval algorithms. It is important to recognise that the BSDF is rather free of structure in both the wavelength and viewing dimensions, unlike the individual absolute radiance and irradiance calibrations.

During the on-ground calibration of the OMI instrument the radiance earth mode and the irradiance sun mode and the instrument BSDF were radiometrically calibrated in absolute sense under flight representative thermal vacuum pressure and temperature conditions (265 K) for the nominal viewing geometry. The viewing angle dependency of the above parameters had to be measured under ambient environmental conditions.

The aluminium on-board diffusers introduce spectral features in the irradiance signal. The features result from both the surface structure of the diffusers and from white light interference caused by the diffuser surface. They interfere with trace gas absorption structures in the earth reflectance spectrum and thereby hinder the retrieval of the column densities of these gases. To reduce these features a new type of volume diffuser was developed that has much better spectral feature behaviour. Scattering by three surfaces effectively reduces the interference effects.

The pre-flight measured absolute radiance and irradiance sensitivities of the OMI instrument at flight representative thermal vacuum conditions for central nadir viewing angle are shown in fig. 3. The enhanced sensitivity of the UV1 spectral channel that is achieved by scaling down the channel both in the spectral and in the spatial dimension is clearly visible in the plot.

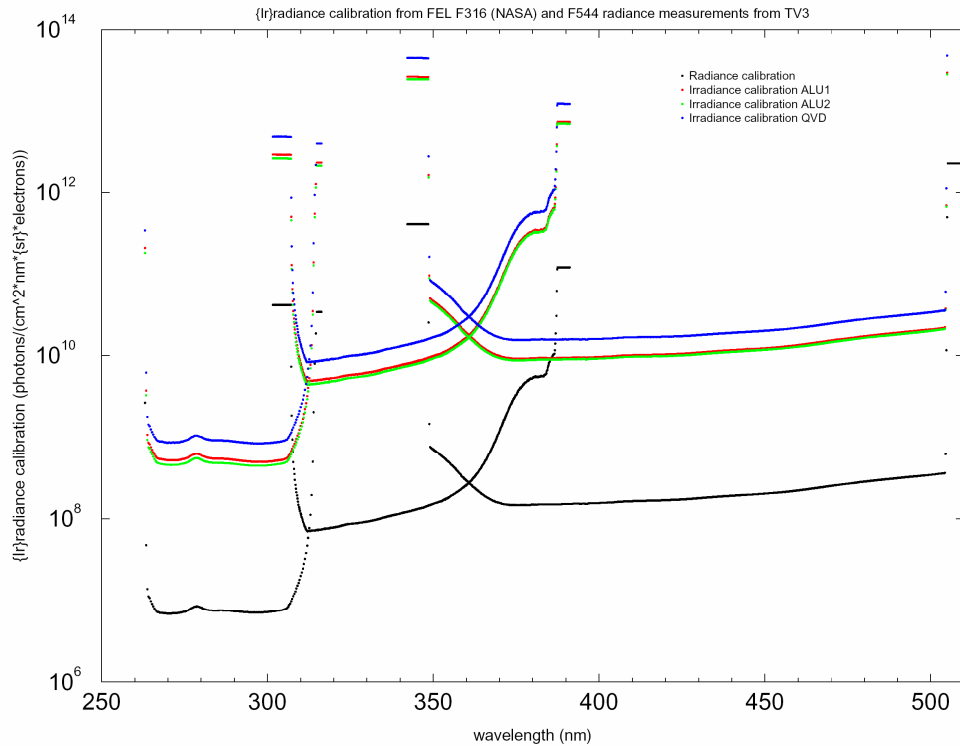


Fig. 3: The absolute radiance calibration of the OMI instrument for the central nadir viewing direction, measured at flight representative thermal vacuum pressure and temperature environmental conditions (black curve). The enhanced sensitivity in the UV1 spectral channel results from scaling down the channel by a factor two in both the spectral and the spatial dimension. The optical channel boundaries are at about 305 and 370 nm. The irradiance sensitivities are shown in red (weekly aluminium diffuser), green (monthly aluminium diffuser) and blue (quartz volume diffuser), also for the central nadir viewing direction.

The OMI instrument BSDF for nadir zero degrees measured at flight representative thermal vacuum conditions is presented in fig. 4 for all three on-board diffusers. The BSDF curve for the quartz volume diffuser is approximately a factor two lower than the BSDF curves for the two aluminium diffusers, as a result of the lower reflectivity efficiency of the quartz volume diffuser. A wavelength dependent BSDF difference between both aluminium diffusers of up to 15% is measured. The spectral structure in the BSDF of the aluminium diffusers above 400 nm originates from the spectral diffuser features. Such features are far less pronounced in the volume diffuser results. The figure shows that the BSDF is a continuous function in wavelength, also across the optical channel boundaries. This behaviour is as expected, and is in contrast to the behaviour of the radiance and irradiance calibration parameters across the channel boundaries, as shown in fig. 3.

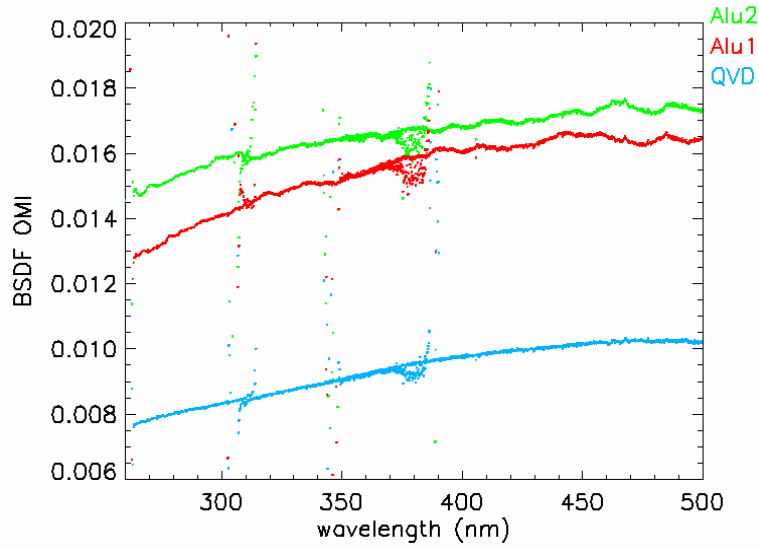


Fig. 4: OMI instrument BSRF in 1/sr for nadir zero degrees viewing angle measured at thermal vacuum environmental conditions for all three on-board reflection diffusers. The result for the volume diffuser is the bottom line.

Fig. 5 shows the resulting OMI instrument BSRF as measured on the ground for the UV2 channel. It can be seen that the result is largely structureless in both the wavelength and viewing dimensions (compare for example for the wavelength dimension to fig. 3). Validation of the BSRF on in-flight earth reflectance measurement data is ongoing.

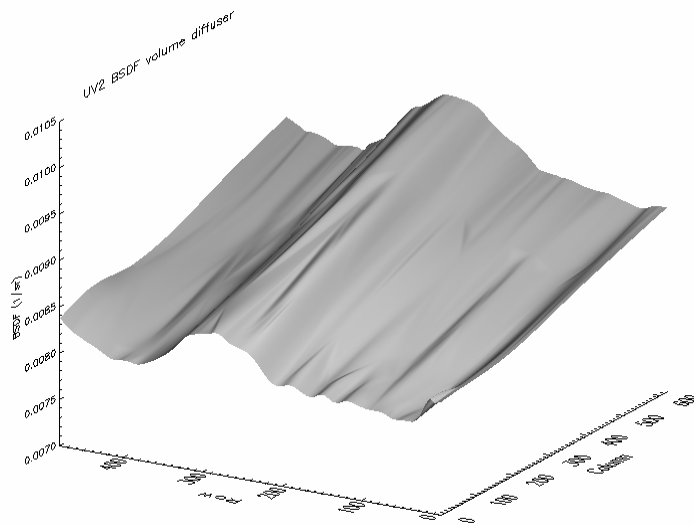


Fig. 5: OMI instrument BSRF for the quartz volume diffuser as a function of column (wavelength) and row (viewing direction) for the UV2 channel (307-383 nm) for nominal azimuth and elevation angles. The central nadir viewing direction corresponds to row 288. Wavelengths increase with increasing column number.

Fig. 6 shows the solar irradiance spectrum as measured in flight over the quartz volume diffuser with binning factor 8 for binned row 33 on 8 February 2005. This spectrum can be compared to a literature high-resolution solar spectrum<sup>7</sup> convolved with the OMI spectral slit function. The OMI spectral slit function was measured very accurately on the ground using a dedicated measurement setup and analysis method, which will not be explained in detail here.<sup>8</sup> The wavelength and viewing angle dependencies of the spectral slit functions were also calibrated accurately. The convolved

spectrum is not shown in fig. 6, because it nearly coincides with the measured spectrum. The ratio of two such spectra is shown in fig. 7 for orbit 2465 of 31 December 2004. From this ratio a couple of observations can be made.

Firstly, the residual Fraunhofer structures are comparatively small, although the results can certainly be optimised further in this respect. The figure shows that the convolution of the high-resolution literature solar spectrum<sup>7</sup> with the measured spectral slit functions reproduces the measured solar Fraunhofer structures well, which indicates that both the literature solar spectrum and the slit functions are accurate. It further shows that the wavelength calibration attached to the measured solar spectrum is accurate to typically a few hundredths of a pixel. This wavelength calibration is based on the measured solar spectrum and the employed algorithm is producing accurate spectral calibration results. Further optimisation in the mentioned areas is planned. Secondly, 1-2% residual structure is observed, especially in UV1 and in the overlap region between UV1 and UV2 at about 305 nm. Also the VIS channel shows some residual structure. This suggests that the wavelength dependence of the absolute radiance and irradiance calibration needs to be revisited and optimised. This needs to be done in a way that no wavelength dependent structure is introduced in the ratio of the two, i.e. the instrument BSRF. Thirdly, the VIS channel seems to be about 2% too high as a whole as compared to the other channels and to the reference solar spectrum. Despite the possibilities for further improvement, the accuracy of the results shown in figs. 6 and 7 is as expected, given the complexity of the OMI design and calibration.

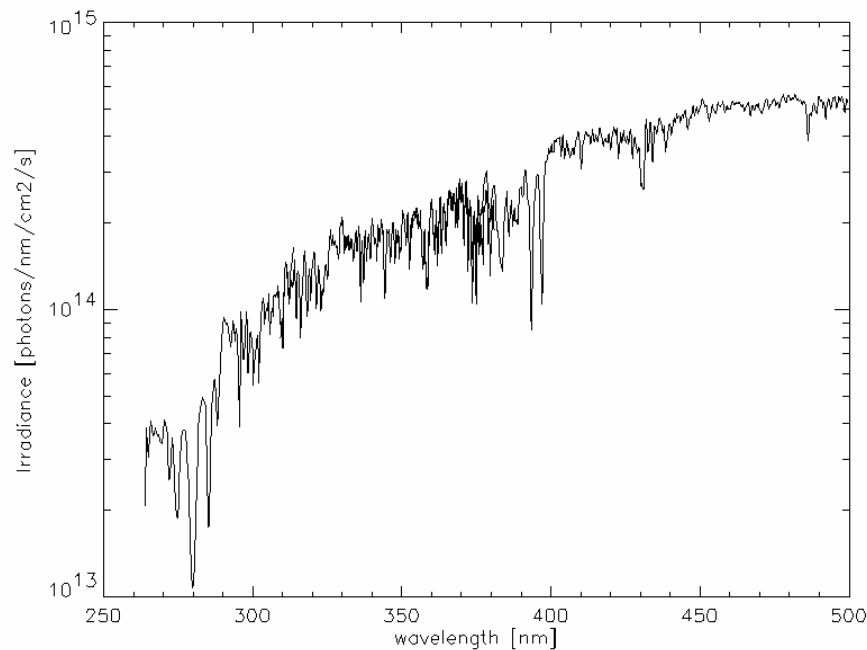


Fig. 6: Measured solar spectrum over the quartz volume diffuser with binning factor 8 for row 33 (orbit 3031, 8 February 2005).

In-flight WLS measurements have been employed to investigate the in-orbit radiometric stability of the OMI instrument during the first year in flight. Fig. 8 shows the relative radiometric stability for the UV1, UV2 and VIS channel averages as a function of time. For each date the signal from a lamp measurement is divided by the signal from a lamp measurement obtained on 20 August 2004, about one month after launch. The results as shown are representative also for smaller areas on the CCD detectors (i.e. wavelengths and viewing directions). Apart from some lamp settling and thermal effects during the first 100 days after launch, the figure shows a change of about 1%, which occurred mainly in the time period May-July 2005. It is currently under investigation whether this change has to be attributed to a decrease in the lamp output or to a decrease in efficiency of other optical components. The accuracy of the ratio from two lamp measurements is about 0.5%.

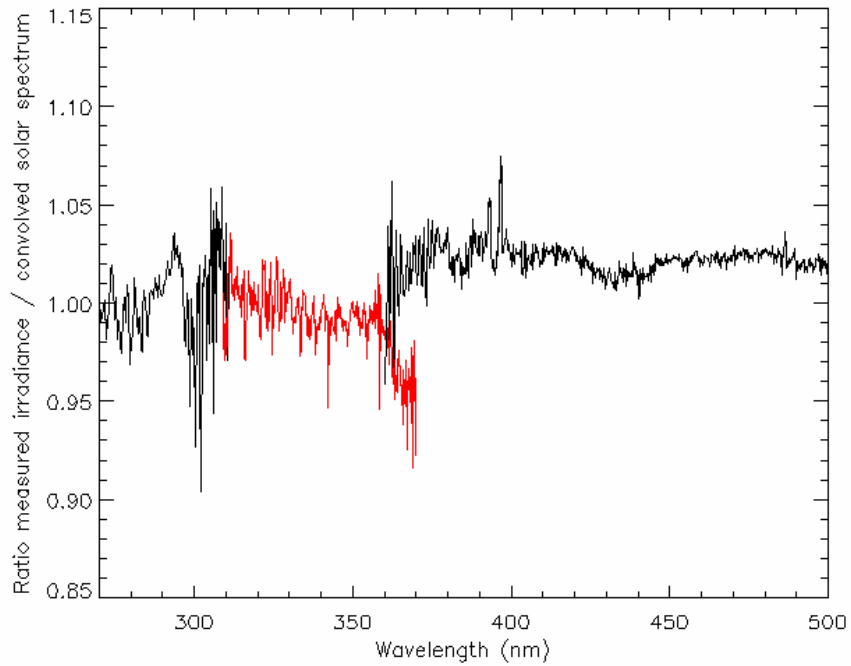


Fig. 7: Ratio of solar irradiance measurement over the quartz volume diffuser with binning factor 8 (orbit 2465, 31 December 2004) and the high-resolution solar reference spectrum convolved with the measured OMI spectral slit function. The UV2 channel is shown in red for clarity.

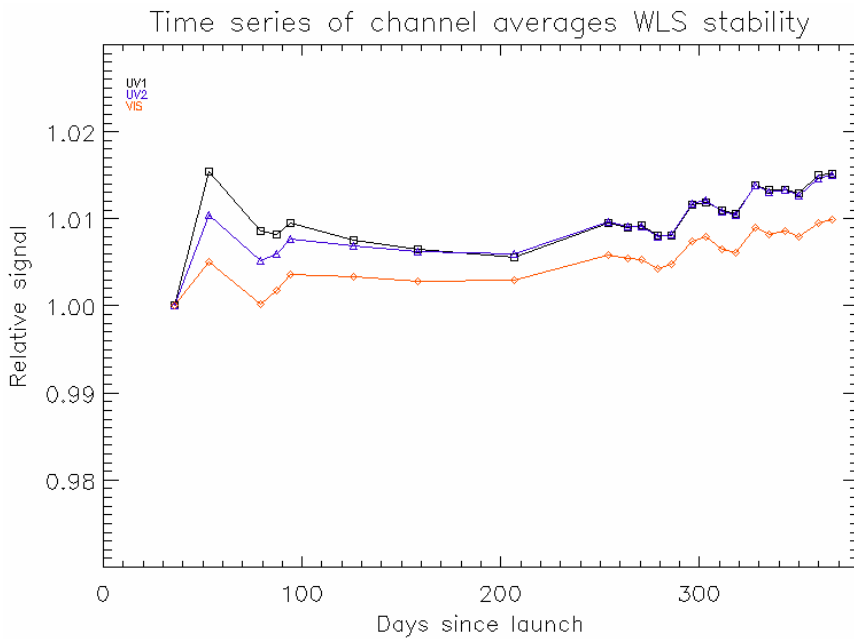


Fig. 8: Instrument optical stability as measured with the internal white light source from launch plus 36 days (20 August 2004) to launch plus one year (17 July 2005) for UV1 (top line), UV2 (middle line) and VIS (bottom line).

## 4. SPECTRAL CALIBRATION

The in-flight wavelength calibration for OMI is performed by use of the Fraunhofer lines in the sun spectra and Earth spectra. During the on-ground calibration spectral calibration data have been obtained by illumination of the calibration port (see section 2) with a dedicated optical stimulus equipped with a PtCrNeAr hollow-cathode spectral light source. Illumination via the calibration port ensures homogeneous filling of the entrance slit and thus instantaneous complete illumination of all viewing directions on the CCD detectors. It was verified that the different optical ports, i.e. sun port, nadir port and calibration port yield the same spectral calibration data and spectral slit function calibration data. The positions of the spectral lines are known to an accuracy of better than 0.01 pixel, but the final accuracy of the spectral calibration from the spectral line source is only about 0.1 pixel, because spectral line blends and line distribution over the wavelength range prevent a higher accuracy.

The wavelength calibration of the OMI instrument is given by:

$$\lambda_{ij} = \sum_{k=0}^N c_{kj} \cdot i^k \quad (1)$$

where  $i$  is the column number,  $j$  the row number and  $c_{kj}$  are the wavelength calibration polynomial coefficients.  $N$  is the order of the polynomial, which is typically 4 for the UV1, UV2 and VIS subchannels.

The in-flight spectral calibration is applied by the 0-1 data processor to Earth and sun measurements. Per subchannel a number of fitting windows are defined. In each window the measured spectrum is compared and fitted to a high-resolution literature solar spectrum<sup>7</sup> convolved with the spectral slit function, which has been calibrated accurately on the ground.<sup>8</sup> The non-linear fitting process determines the wavelength scale of the window by shifting and squeezing the measured spectrum until an optimal match is obtained. For the Earth spectra ozone absorption and the atmospheric Ring effect are also taken into account. Subsequently, a polynomial (typically of order 4) is fitted through this set of predefined and optimized windows per subchannel. This defines the wavelength calibration per subchannel and per row. This algorithm is performed for each binned or unbinned row available in the sun measurement, but only for the central nadir row for Earth measurements to keep the total orbit processing time within limits. Typical accuracies of the wavelength calibration that are obtained using the above algorithm on in-flight measurement data are for the solar spectra about 0.02 px in UV1, UV2 and VIS and for the Earth spectra 0.04-0.05 px in UV1, UV2 and VIS, as can be seen from fig. 9.

The results of the in-flight wavelength calibration on Earth spectra along complete orbits show that wavelength shifts of several hundredths of a pixel occur when the signal intensity changes, i.e. when ground scene changes in the flight direction occur, particularly in case of clouds. This holds particularly for the UV2 and VIS channel, but not for the UV1 channel, because for wavelengths below 305 nm the ground is not seen and scene-to-scene variability is much less. The effect can be explained in terms of partial or non-uniform filling of the entrance slit in the flight direction, which is also the spectral dispersion direction. This influences the shape of the spectral slit function, which is narrowed and shifted with respect to the situation corresponding to complete uniform entrance slit filling. It turns out that it is possible to correct for this effect, which is the main contributor to the inaccuracies as quoted above, by using the so-called small-pixel column data in the UV2 and VIS channel, for which a number of data points equaling the coadding factor are available for each read-out of the CCD detectors. For example, a complete binned image (60 rows) is read out every 2 seconds with an exposure time of 0.4 seconds and a coadding factor of 5. Small pixel data, one column in the UV2 channel and one in the VIS channel, are available at a higher frequency, in the example above 5 small pixel data points per 2 seconds, equal to the coadding factor. The correction for the observed wavelength shift makes use of the correlation that exists between the observed wavelength shifts and the gradients in the small-pixel column data. Fig. 10 shows an example of this correlation in the VIS channel for an arbitrary orbit. By applying the wavelength correction for changing scenes in the 0-1 data processing the accuracy of the in-flight wavelength calibration of Earth shine spectra approaches 0.01 px, which is the goal accuracy for the in-flight wavelength calibration.

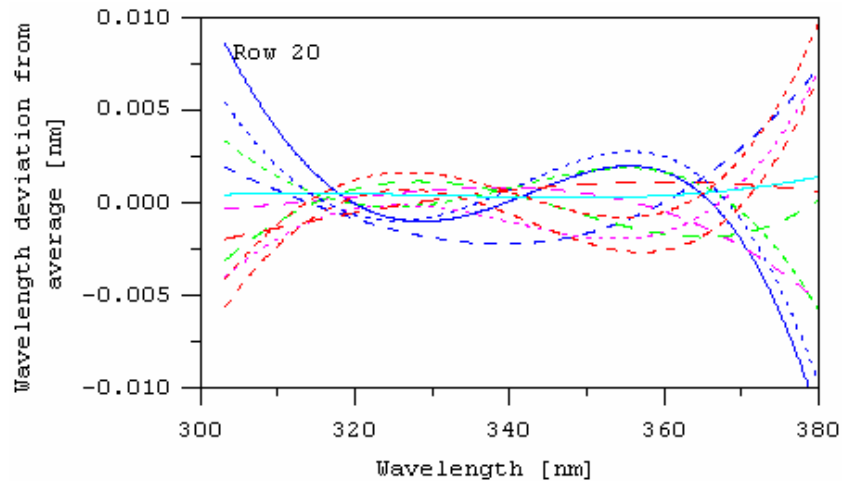


Figure 9: Differences between wavelength scales obtained from 10 single independent volume diffuser sun measurements, for several rows in UV2, showing the reproducibility of the wavelength calibration from the in-flight solar measurement data.

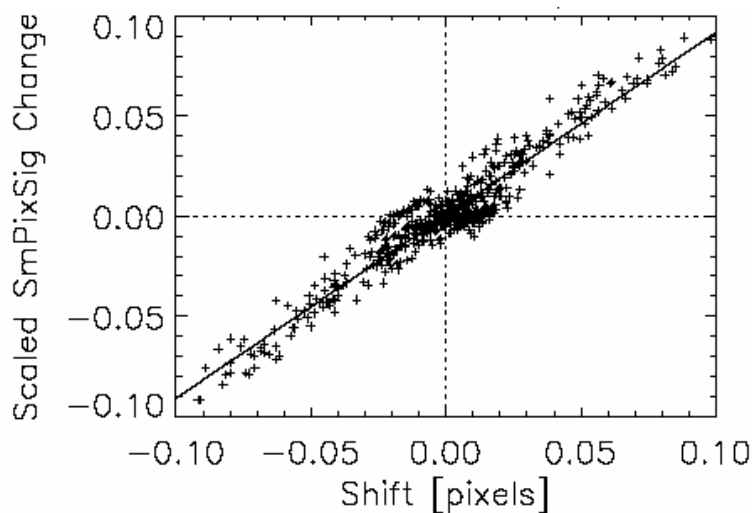


Fig. 10: Correlation for earth shine spectra between wavelength shifts close to cloud transitions and gradients in small pixel column readouts for the VIS channel. This effect is attributed to partial slit illumination at inhomogeneous ground scenes and is corrected in the 0-1 data processor using a correlation as shown. In the figure the correlation coefficient is 0.96, the slope is 0.92.

## 5. CONCLUSIONS

A number of in-flight calibration and performance results of the Ozone Monitoring Instrument OMI, successfully launched on 15 July 2004 on the EOS-AURA satellite, have been presented and discussed. The OMI instrument works flawlessly in orbit and the performance is as expected from on-ground testing. A number of details on the pre-launch and post launch radiometric calibration were discussed. These results show that the radiometric calibration in

comparison to the high-resolution literature solar irradiance data convolved with the calibrated spectral slit function is understood and as expected in terms of offsets and spectral structure. The instrument shows no signs of optical degradation over the wavelength range 264-504 nm during the first year after launch. The in-flight spectral calibration was discussed. After correction on the Earth measurement data in the 0-1 data processing for the inhomogeneous illumination of the spectrometer's entrance slit in UV2 and VIS as a result of inhomogeneous ground scenes (clouds), the accuracy of the spectral calibration approaches 0.01 pixel, which is the goal accuracy. In general, more detailed analysis work on the available in-flight measurement data is required to fully understand the in-flight calibration and performance behaviour of the OMI instrument.

## REFERENCES

1. R. D. McPeters, P. K. Bhartia, J. K. Arlin, J. R. Herman, C. G. Wellemeyer, C. J. Seftor, G. Jaross, O. Torres, L. Moy, G. Labow, W. Byerly, S. L. Taylor, T. Swissler, R. P. Cebula, 1998: Earth Probe Total Ozone Mapping Spectrometer (TOMS) Data Products User's Guide. NASA Tech. Publ. 1998-206895.
2. U. Platt, "Differential Optical Absorption Spectroscopy (DOAS)", in *Air Monitoring by Spectroscopic Techniques*, edited by M.W. Sigrist, pp. 27-84, John Wiley & Sons, New York, 1994.
3. J. M. C. Plane and N. Smith, "Atmospheric Monitoring by Differential Optical Absorption Spectroscopy in Environmental Science", *Adv. in Spectroscopy*, v 24, edited by R.J.H. Clark and R.E. Hester, 1994.
4. R. Dirksen, M. Dobber, P. Levelt, G. H. J. van den Oord, G. Jaross, M. Kowalewski, G. H. Mount, D. Heath, E. Hilsenrath and J. de Vries, "The on-ground calibration of the Ozone Monitoring Instrument from a scientific point of view", Proceedings SPIE 10<sup>th</sup> International Symposium Remote Sensing, Barcelona (Spain), 8-12 September 2003, vol. 5234, pp. 400-410, published by SPIE, Bellingham, Washington 98227-0010, U.S.A.
5. M. Dobber, R. Dirksen, P. F. Levelt, G. H. J. van den Oord, G. Jaross, M. Kowalewski, G. H. Mount, D. Heath, E. Hilsenrath and R. Cebula, "Ozone Monitoring Instrument flight-model on-ground and in-flight calibration", International conference on Space Optics (ICSO). Toulouse (France), 30 March – 2 April 2004, European Space Agency (ESA) publication SP-554, Noordwijk, The Netherlands.
6. J. de Vries, G. H. J. van den Oord, E. Hilsenrath, M. te Plate, P. Levelt and R. Dirksen, "Ozone Monitoring Instrument (OMI)", Proceedings of SPIE, San Diego (U.S.A.), 1-3 August 2001, Imaging Spectrometry VII, M.R. Descour and S.S. Chen editors, vol. 4480, pp. 315-325, published by SPIE, Bellingham, Washington 98227-0010, U.S.A.
7. R. L. Kurucz, I. Furenlid, J. Brault and L. Testerman, Solar flux atlas from 296 to 1300 nm, National Solar Observatory, Sunspot, New Mexico, 240 pp, 1984.
8. M. Dobber, R. Dirksen, R. Voors, G.H. Mount, P. Levelt, "Ground-based zenith sky abundances and in situ gas cross sections for ozone and nitrogen dioxide with the Earth Observing System Aura Ozone Monitoring Instrument", *Applied Optics*, vol. 44, no. 14, 2846-2856, 2005.